BIOCHEMISTRY
including biophysical chemistry & molecular biology

Article

pubs.acs.org/biochemistry

Crystal Structure of Glucokinase Regulatory Protein

Alexander Pautsch,*[,†] Nadja Stadler,[†] Adelheid Löhle,[†] Wolfgang Rist,[∥] Adina Berg,[⊥] Lucia Glocker,[‡] Herbert Nar,[†] Dirk Reinert,[†] Martin Lenter,[§] Armin Heckel,[⊥] Gisela Schnapp,[†] and Stefan G. Kauschke[‡]

[†]Departments of Lead Identification and Optimization Support, [‡]CardioMetabolic Diseases Research, [§]CNS Diseases Research, [∥]Drug Discovery Support, [⊥]BP Process Science, and [@]Medicinal Chemistry, Boehringer Ingelheim Pharma GmbH & Company KG, Biberach an der Riss, Germany

Supporting Information

ABSTRACT: Glucokinase (GK) plays a major role in the regulation of blood glucose homeostasis in both the liver and the pancreas. In the liver, GK is controlled by the GK regulatory protein (GKRP). GKRP in turn is activated by fructose 6-phosphate (F6P) and inactivated by fructose 1-phosphate (F1P). Disrupting the GK−GKRP complex increases the activity of GK in the cytosol and is considered an attractive concept for the regulation of blood glucose. We have determined the crystal structure of GKRP in its inactive F1P-bound form. The binding site for F1P is located deeply buried at a domain interface, and H−D exchange experiments confirmed that F1P and F6P compete for this site. The structure of the inactive GKRP−F1P complex provides a starting point for understanding the mechanism of fructose phosphate-dependent GK regulation at an atomic level.

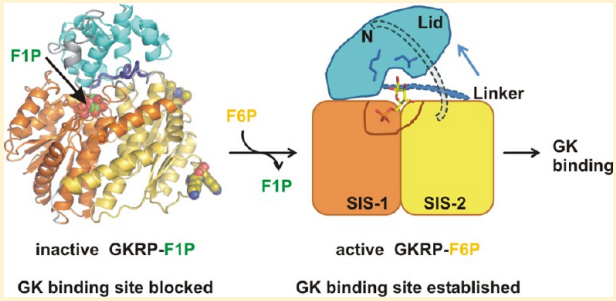

Glucokinase (hexokinase IV, GK) plays a major role in the regulation of blood glucose homeostasis because of its important role as the dominant glucose phosphorylating enzyme in both the liver and the pancreas, its major sites of expression.[1] GK functions as a key regulator of both hepatic glucose metabolism (hepatic glucose uptake, hepatic glucose output) as well as of pancreatic insulin secretion. Its sigmoidal activation curve with glucose, a unique feature among the family of hexokinases, allows a fast and pronounced response of activity to fluctuations in plasma glucose levels.[1,2] Crystal structures have revealed that GK can cycle between at least two conformations. In the presence of ligands and/or synthetic activators, GK was crystallized in a "closed", active conformation.[3,4] In the absence of either glucose or activator, GK adopts a "super-open", inactive apo conformation.[4] Moreover, the existence of an intermediate "open", active conformation was proposed on the basis of a comparison with hexokinase I.[4] It is hypothesized that GK is shifted toward the active conformations as a function of D-glucose concentration and that the reversible transition between conformations is slower than the catalytic cycle,[5] resulting in a unique positive kinetic cooperativity with glucose.[6]

In the liver, GK is regulated not only by the presence of its substrate glucose but also by the 68 kDa regulatory protein GKRP (glucokinase regulatory protein) that inhibits GK in a competitive manner with respect to glucose.[7] In the presence of low glucose levels, GK is bound to GKRP, forming an inactive complex, which is predominantly localized in the nucleus. When glucose levels are replenished, e.g., by feeding, the inactive GK−GKRP complex dissociates and GK translocates into the cytosol, its site of action.

In addition to the impact of glucose itself on the dissociation of the GK−GKRP complex, likely via affecting GK directly, different fructose phosphates play an important role in increasing the respective probabilities of both the assembly of the inactive GKRP−GK nuclear complex and its dissociation.[8] While it could be shown that the binding of fructose 6-phosphate (F6P) to GKRP increases its affinity for GK thereby favoring the inactive complex, the binding of fructose 1-phosphate (F1P) or its analogue sorbitol phosphate to GKRP, on the other hand, destabilizes the complex and shifts the equilibrium of total GK to the free and active form in the cytosol.[9]

Increasing GK activity through small molecule activators (GKAs) is under intense investigation both in preclinical phases and in clinical phases as a novel antidiabetic principal.[6,10] The orthogonal strategy, disrupting the inactive GK−GKRP complex, increases the level of GK in the cytosol and its activity.[11,12] Although this theoretically is an attractive concept, no progress in this direction has been reported.

Our current knowledge of the molecular details of the GK−GKRP complex is limited and originates mainly from indirect evidence based on enzymatic[13] and biophysical[14] experiments. While first site-directed mutagenesis efforts that aimed to investigate selected amino acids and their potential involvement in fructose binding and their impact on GK−GKRP complex formation indicated at least in part overlapping binding sites for fructose phosphates on GKRP,[8] there is a lack of in-depth

Received: January 22, 2013
Revised: April 12, 2013
Published: April 26, 2013

 © 2013 American Chemical Society

Table 1. Data Collection, Phasing, and Refinement

	F1P-1	EuAc3	F1P-2	phosphate
		Data Collection[a]		
wavelength (Å)	1.00	1.30	0.960	0.910
space group	$P2_12_12_1$	$P2_12_12_1$	$P2_12_12_1$	$P2_12_12_1$
unit cell dimensions [*a*, *b*, *c* (Å)]	60.6, 72.3, 137.4	60.8, 71.8, 137.3	61.0, 72.3, 136.9	60.8, 72.2, 138.0
resolution (Å)	50−1.67	72−1.90	72−1.47	69−1.92
highest-resolution shell (Å)	1.74−1.67	1.98−1.90	1.53−1.47	1.98−1.92
no. of observed reflections	249597	602957	347484	306781
no. of unique reflections	70207	48118	102068	47132
completeness (%)	99.1 (99.1)	99.9 (99.9)	98.6 (98.2)	99.9 (100.0)
R_{sym} (%)[b]	5.1 (38.0)	9.5 (44.4)	5.1 (39.8)	9.8 (44.1)
$\langle I/\sigma(I)\rangle$	15.8 (3.3)	20.6 (6.7)	14.7 (3.9)	17.0 (6.5)
		Phasing		
phasing power[c]				
isomorphous acentric		0.611		
isomorphous centric		0.553		
anomalous acentric		0.910		
figure of merit (centric/acentric)		0.16/0.24		
		Refinement		
R factor[d] (%)	not refined	not refined	16.0	16.0
R_{free}[e] (%)			17.7	18.6
no. of refined atoms			5357	5086
protein			4640	4635
solvent			700	446
ligand			17	5
average *B* factor (Å^2)			18.6	18.1
rmsd				
bond lengths (Å)			0.008	0.008
bond angles (deg)			0.96	0.98
Ramachandran statistics (%)				
favored			98.6	98.1
allowed			1.1	1.5
outliers			0.3[f]	0.3[f]

[a]Values in parentheses are for the highest-resolution shell. [b]$R_{sym} = \sum_{hkl}\sum_i|I_i - \langle I\rangle|/\sum_{hkl}\sum_i I_i$. [c]Phasing power = F_H/(lack of closure). [d]*R* factor = $\sum_{hkl}||F_{obs}| - k|F_{calc}||/\sum_{hkl}|F_{obs}|$. [e]$R_{free}$ was calculated using 5% of the data excluded from refinement. [f]The three Ramachandran outliers are well-defined in the electron density.

details on either the molecular structure of GKRP, the precise binding sites of its endogenous regulators, or the underlying regulatory mechanisms. As a first step in understanding the molecular mechanism of fructose phosphate-dependent regulation of GK, we have determined the crystal structure of GKRP in its inactive F1P-bound form.

MATERIALS AND METHODS

Molecular Biology. The gene encoding human GKRP (SWISS-Prot entry Q14397, residues 1−625) was codon-optimizied for expression in insect cells and synthesized at GENEART (Regensburg, Germany). The cDNA was flanked by attB1 and attB2 sites. The Gateway system was used to perform cloning into pDONR221 and subsequently into the pDEST8 vector (Invitrogen). The resulting open reading frame encodes human GKRP 1−625 and a C-terminal LEHHHHHH tag. This construct is termed $GKRP_{WT\text{-}His}$. The $GKRP_{WT\text{-}His}$ K326T/K327T mutant ($GKRP_{K326}$) is identical to $GKRP_{WT\text{-}His}$ except for amino acids K326 and K327, which were mutated to threonine by using the gene synthesis approach at GENEART. After the corresponding bacemids had been constructed via the BAC-to-BAC system (Invitrogen), the proteins were expressed in High FIVE cells for 72 h at 27 °C. The cells were harvested by centrifugation and frozen at −70 °C.

Protein Purification. Frozen cells were thawed, resuspended in lysis buffer [25 mM Hepes (pH 8), 0.1 mM $MgCl_2$, 500 mM NaCl, Complete EDTA-free protease inhibitor (Roche Diagnostics, one tablet/50 mL), 0.2 mM DTT, and 3 μg/mL DNase], and broken by one freeze−thaw cycle. The lysate was centrifuged for 60 min at 20000*g*. The supernatant (400 mL) was incubated with 9 mL of Ni-NTA agarose beads in buffer A [50 mM Na_2HPO_4 (pH 8.0) and 500 mM NaCl] for 60 min at 4 °C. Beads were washed with 40 mL of buffer A and subsequently with 2% buffer B [50 mM Na_2HPO_4 (pH 7.0), 500 mM NaCl, 0.5 M imidazole, and 5 mM DTT] in buffer A until the absorbance at 280 nm (A_{280}) of the eluate returned to baseline (approximately 40 mL). After the sample had been washed, GKRP was eluted from the beads in 20 mL of buffer B. The eluted protein was concentrated and further purified by size exclusion chromatography (Superdex 200, Amersham) in buffer S [100 mM Hepes (pH 7.4), 200 mM KCl, 1 mM $MgCl_2$, and 2 mM DTT]. Mutants and other variants were expressed and purified following the same protocol.

Enzymatic Assay of Glucokinase Regulatory Protein. The effect of GKRP on glucokinase activity was determined using the glucose-6-phosphate dehydrogenase coupled assay at room temperature by a modification of methods described

dx.doi.org/10.1021/bi4000782 | *Biochemistry* 2013, 52, 3523−3531

previously.[7,15] The final reaction mixture contained 150 mM KCl, 100 mM Hepes, 1 mM ATP, 1 mM $MgCl_2$, 2 mM $NADP^+$, 2 mM dithiothreitol (pH 7.4), 5 units/mL glucose-6-phosphate dehydrogenase, 0.5 mg/mL BSA, 10 mM glucose, 6 μM F6P, 15 nM human liver glucokinase, and 100 nM GKRP. The enzymatic reaction was started by the addition of ATP and glucose. The increase in the optical density was measured at a wavelength 340 nm over 10 min. From these kinetic data, the slope was calculated and graphically depicted.

H−D Exchange. Amide hydrogen exchange was initiated by a 20-fold dilution of 30 pmol of GKRP with or without ligand into D_2O containing 100 mM Hepes (pH 7.4), 200 mM KCl, 100 mM $MgCl_2$, and 2 mM DTT and incubated at room temperature. After various time points (10 s, 1 min, and 30 min), the exchange reaction was quenched by decreasing the temperature to 0 °C and the pH to 2.5 with quench buffer [500 mM KH_2PO_4/H_3PO_4 (pH 2.5), 2 M urea, and 2 mM TCEP]. Quenched samples were directly injected into an HPLC setup and analyzed on an electrospray ionization quadrupole time-of-flight mass spectrometer (QSTAR XL, Applied Biosystems) as described previously.[16] The HPLC setup contained a column (2 mm × 20 mm) packed with Poroszyme immobilized pepsin (Applied Biosystems, Darmstadt, Germany). The resulting peptides were trapped on a 0.5 mm × 5 mm reversed-phase column (Reprosil-Pur C8) and eluted from the trap column over a 0.5 mm × 100 mm Reprosil-Gold C8 analytical reversed-phase column (Dr. Maisch, Ammerbuch-Entringen, Germany) with an 8 min gradient directly into the electrospray source. The digestion, desalting, and elution required <10 min. The whole setup was immersed in an ice bath to minimize back-exchange. Peptic peptides of GKRP were identified on the basis of their MS/MS spectra. The deuterium content of the peptides was calculated by using the average mass difference between the isotopic envelopes of the deuterated and undeuterated peptides.

Crystallization. Screens for initial crystallization conditions were performed with commercial sparse matrix screens at two temperatures (4 and 20 °C) in the absence or presence of fructose 1-phosphate. Prior to crystallization, the $GKRP_{K326}$−F1P complex was prepared by incubating $GKRP_{K326}$ at 12−16 mg/mL in 25 mM Hepes (pH 7.4), 50 mM KCl, 1 mM $MgCl_2$, 2 mM DTT, and 5 mM F1P for 1 h at 4 °C. One initial crystallization condition for the $GKRP_{K326}$−F1P complex was identified (JCSG+ screen, condition 59, Qiagen), which had already yielded diffraction quality crystals. Typical crystallization drops were formed at 20 °C using the sitting drop vapor diffusion method by mixing 1 μL of the $GKRP_{K326}$−F1P complex and 1 μL of a reservoir solution consisting of 14% PEG 8000, 20% glycerin, 0.16 M calcium acetate, and 0.08 M cacodylate (pH 6.5). Crystals were flash-frozen in a 100 K nitrogen stream, with the mother liquor serving as the cryoprotectant. $GKRP_{K326}$ in a complex with phosphate ($GKRP_{K326}$−P) was crystallized as described for the $GKRP_{K326}$−F1P complex, but without the addition of 5 mM F1P to the crystallization buffer. The reservoir solution consisted of 20% PEG 3350 and 0.1 M Tris (pH 8.0). Phosphate was not explicitly added, but residual phosphate from the previous Ni-NTA purification step remained bound to the protein (see below).

Data Collection, Sructure Solution, and Refinement. All diffraction data were collected at 100 K on the PX-1 beamline at the SLS (Villigen, Switzerland) and processed with XDS.[17] The data processing statistics are listed in Table 1. An initial high-resolution data set [F1P-1 (Table 1)] was used for molecular replacement trials and SIRAS phasing. For initial molecular replacement trials, we used models identified with the help of the hhpred server,[18] but no clear solution could be identified. The structure of the $GKRP_{K326}$−F1P complex was determined with the SIRAS method. For derivatization, we soaked a crystal of the $GKRP_{K326}$−F1P complex for 3 days in artificial mother liquor, in which the calcium acetate was exchanged with 160 mM $EuAc_3$. Identification of the heavy atom substructure, phasing, and density modification were performed using autoSharp (Global Phasing Ltd.) and SHELXD.[19] The model of $GKRP_{K326}$ was semiautomatically built with ARP/wARP.[20] Subsequently, missing residues as well as fructose 1-phosphate were manually built using Coot,[21] and the resulting model was improved by iterative rounds of manual rebuilding and refinement with autoBuster (Global Phasing Ltd.). The final refinement was performed against data set F1P-2 that originated from a crystal that had been unsuccessfully soaked with $AuCl_3$ for derivatization. The final model consists of residues 6−606 of $GKRP_{K326}$, one fructose 1-phosphate molecule, one Ca^{2+} ion, and 700 water molecules. N- and C-termini as well as a short surface loop (residues 64−68) are disordered. As defined by MolProbity,[22] 98.6% of residues are in the most favored regions of the Ramachandran plot and 1.0% in additionally allowed regions. The structure of the $GKRP_{K326}$−phosphate complex ($GKRP_{K326}$−P) was determined by difference Fourier methods and refined as described above. The final statistics for the models are listed in Table 1, and a representative portion of the final electron density is shown in Figure 3A. PyMOL (DeLano Scientific LLC) was used for figure preparation and structural analysis (rmsd calculations and distance measurements). Coordinates of F6P were taken from Protein Data Bank (PDB) entry 1NUZ and manually placed in the F1P binding site.

RESULTS AND DISCUSSION

Structure Determination. Using an insect cell expression system, we could express human, wild-type, full length GKRP ($GKRP_{WT\text{-}His}$). The resulting protein could be purified in milligram amounts, was homogeneous according to ESI-MS and size exclusion chromatography (data not shown), and could be concentrated to >20 mg/mL. GKRP from two rodent species could be produced analogously (data not shown). It was possible to identify initial crystallization conditions for human and murine GKRP in complex with F1P, but in both cases, the crystals were conjoined, did not diffract to better than 4 Å resolution, and could not be optimized to a quality sufficient for structure solution. To explore whether N- and/or C-terminally unstructured regions were detrimental to the formation of better ordered crystals, we then used truncated variants (data not shown) of human GKRP based on sequence conservation, secondary structure, and domain prediction[18,23] as well as limited proteolysis. Again, the proteins could be expressed in large amounts, but diffraction quality crystals could not be obtained. A similar result was observed when we modified the affinity tag in the context of full-length human GKRP. Whereas protein with an N-terminal His_6 affinity tag was unstable, two constructs with altered C-terminal affinity tags could be homogeneously purified in large amounts but yielded the same malformed crystal habitus as $GKRP_{WT\text{-}His}$ (data not shown). Because the solubility and homogeneity of the protein samples apparently were not the limiting factor for the formation of well-ordered crystals, we decided to explore

dx.doi.org/10.1021/bi4000782 | Biochemistry 2013, 52, 3523−3531

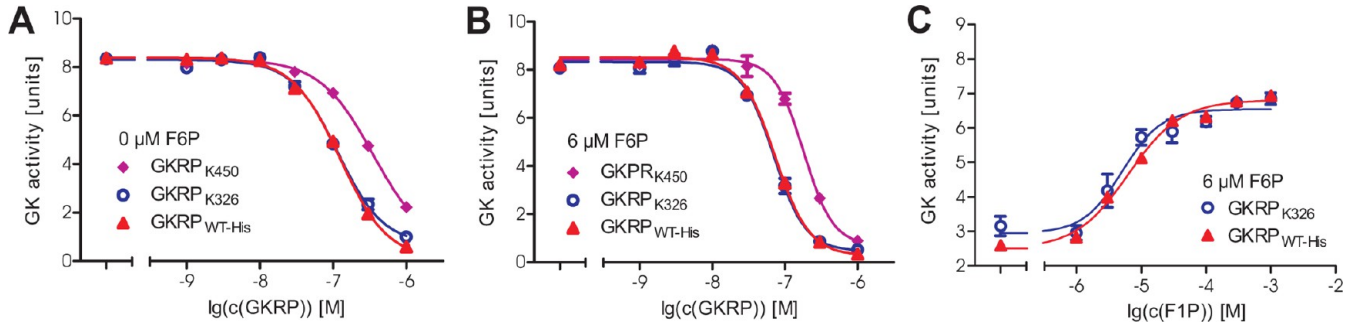

Figure 1. Biochemical characterization of $GKRP_{WT-His}$, $GKRP_{K450}$, and $GKRP_{K326}$. (A) GK inhibition by GKRP (experimental conditions, 15 nM GK and variable amounts of GKRP). (B) GK inhibition by GKRP and F6P (experimental conditions, 15 nM GK, 6 μM F6P, and variable amounts of GKRP). (C) Increase in GK activity upon destabilization of the GK−GKRP−F6P complex by F1P (experimental conditions, 15 nM GK, 100 nM GKRP, 6 μM F6P, and variable amounts of F1P).

surface entropy reduction[24] as a method for increasing crystallization probability. There flexible, charged, and surface-exposed amino acids (Lys, Arg, and Glu) are mutated to small amino acids (Thr, Ser, and Ala) with the intention of rigidifying the protein surface and thereby creating regions more favorable for the formation of crystal contacts. Because no three-dimensional structure of a close GKRP homologue was known to guide the selection of potential surface-exposed residues, we identified lysine rich regions in the primary sequence of human GKRP and expressed five mutants of $GKRP_{WT-His}$, in which lysines were exchanged with threonine. The double mutant K326T/K327T ($GKRP_{K326}$) in complex with fructose 1-phosphate ($GKRP_{K326}$−F1P) finally yielded well-ordered crystals that diffracted to high resolution (Table 1). The $GKRP_{K326}$−F1P complex crystallized in space group $P2_12_12_1$ with one molecule in the asymmetric unit. The phase problem was solved experimentally by the SIRAS method. A model of the $GKRP_{K326}$−F1P complex was refined to a resolution of 1.47 Å with an R_{free} of 17.7% and consists of residues 6−606 of $GKRP_{K326}$ (Table 1).

Biochemical Characterization. Using GK activity as a readout, major biochemical characteristics of wild-type human GKRP were compared with those of different GKRP variants, in particular $GKRP_{K326}$. As found previously,[14,15] recombinant $GKRP_{WT-His}$ alone is capable of inhibiting the apparent GK activity in a dose-dependent manner by inducing an inactive GK−GKRP complex (Figure 1A). When the compound was dosed in excess over GK (final concentration of 15 nM), an almost complete inhibition (>90%) of the apparent GK enzymatic activity was observed, indicating a very pronounced shift of the equilibrium toward the inactive GK−GKRP complex (IC_{50} = 124 ± 9 nM). The addition of 6 μM F6P induces a higher affinity of the F6P-bound GKRP protein for GK binding, as the inhibition of GK activity already occurs at lower GKRP concentrations (IC_{50} = 74 ± 6 nM) (Figure 1B). The effect of F6P on the formation of the inactive GK−GKRP−F6P complex is dose-dependent (data not shown).

The impact of GKRP surface mutants on the formation of the GK−GKRP complex differs. While $GKRP_{K326}$ and a second double mutant, K450T/K451T ($GKRP_{K450}$), both contain two adjacent surface lysine/threonine substitutions, $GKRP_{K326}$ displays wild-type GKRP-like properties concerning its interaction with GK, whereas the ability of $GKRP_{K450}$ to form an inactive GK−GKRP or GK−GKRP−F6P protein complex is impaired (Figure 1A,B). In comparison to wild-type GKRP, $GKRP_{K326}$ is equally capable of decreasing the apparent activity of GK in the reaction mixture by inducing the formation of the inactive complexes both alone and in the presence of 6 μM F6P (IC_{50} = 116 ± 10 and 71 ± 7 nM, respectively). Using the surface mutant $GKRP_{K450}$, it requires ∼3-fold more GKRP mutant protein in the reaction mixture to shift the equilibrium toward the inactive complex. While the K450T and K451T mutations seem to weaken the ability of the protein to form an inactive complex with GK (IC_{50} = 351 ± 58 nM), the binding of F6P itself seems not to be influenced, as 6 μM F6P is capable of promoting the formation of the inactive GK−$GKRP_{K450}$−F6P complex (IC_{50} = 182 ± 18 nM).

The ability of F1P to compete with the binding of F6P as suggested in ref 8 was investigated using both $GKRP_{WT-His}$ and $GKRP_{K326}$. In the presence of 6 μM F6P, increasing concentrations of F1P are able to dose-dependently increase the apparent GK activity in the reaction mixture. The concentrations of F1P needed to drive the equilibrium from the inactive GK−GKRP−F6P complex toward free GK are comparable using either wild-type $GKRP_{WT-His}$ (EC_{50} = 6.28 ± 1.07 μM) or $GKRP_{K326}$ (EC_{50} = 5.08 ± 1.38 μM) (Figure 1C). This indicates that the major functional properties of $GKRP_{K326}$, namely to bind to GK, to function as a regulator of GK activity, and to be regulated by its endogenous regulatory molecules F6P and F1P in a competitive way, are fully retained and are quantitatively equivalent to those of wild-type GKRP in our hands.

Structure of GKRP. GKRP is trilobal in shape (Figure 2). It consists of two topologically identical sugar isomerase (SIS) domains[23] of equal size, herein termed SIS-1 (residues 45−284) and SIS-2 (residues 289−498), capped by an α-helical C-terminal domain (residues 499−606, termed the Lid domain), which in turn is embraced by residues 6−44 of the N-terminus. In the following discussion, secondary structure elements are designated with indices N (N-terminus), A (SIS-1), B (SIS-2), and C (Lid domain) (Figure S1 of the Supporting Information). The SIS domain fold represents the nucleotide-binding motif of a flavodoxin type.[25] Each SIS domain has an $\alpha\beta$ structure and is dominated by a five-stranded parallel β-sheet flanked on either side by α-helices forming a three-layer $\alpha\beta\alpha$ sandwich (Figure 2C). Helices in the loops connecting β-strands run approximately antiparallel to the strands. In addition to this motif, there is an ∼20-residue α-helical extension donated by the N-terminus of each subdomain (αA1, residues 46−59 of SIS-1; αB1, residues 289−307 of SIS-2) that folds over the domain interface and onto the other respective domain. Both SIS domains are related by an approximate 2-fold

dx.doi.org/10.1021/bi4000782 | Biochemistry 2013, 52, 3523−3531

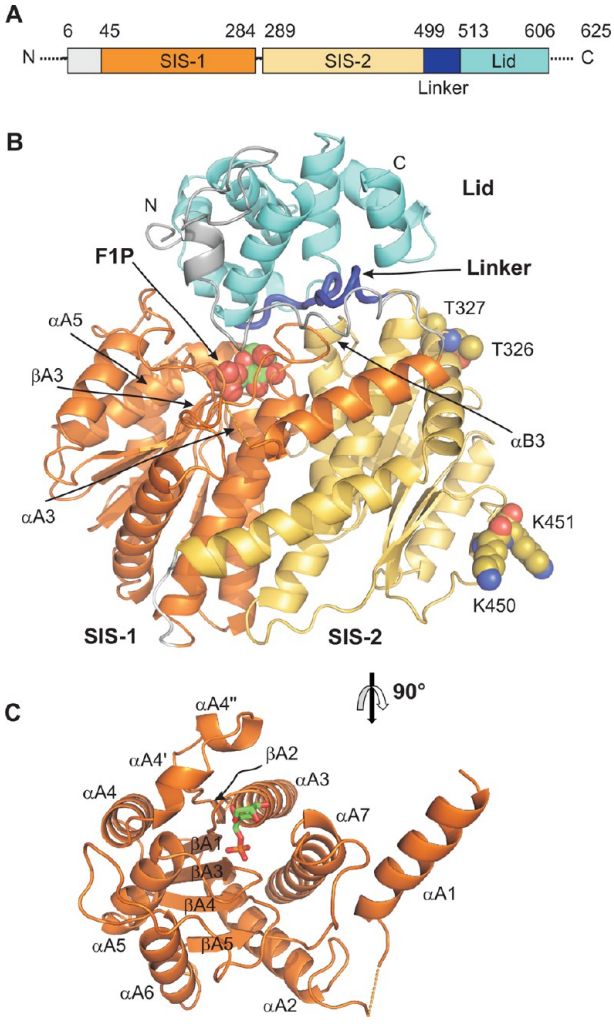

Figure 2. Structure of GKRP. (A) GKRP domain arrangement. (B) Ribbon diagram of $GKRP_{K326}$. The individual domains are colored as in panel A. Ligand F1P and sites probed by mutational analysis are shown as spheres. Selected structural elements involved in F1P binding are labeled. The view is approximately down the pseudo-2-fold axis that relates SIS-1 and SIS-2. (C) Ribbon representation of SIS-1 with all secondary structure elements labeled. The orientation of the SIS-1 domain is related to that in panel B by an ~90° rotation toward the viewer around the image horizontal.

axis going through the SIS domain interface that is built from helices αA1, αA3, and αA7 (SIS-1) and the corresponding helices of SIS-2 (αB1, αB3, and αB7). The two SIS domains can be superimposed with an rmsd of 1.7 Å for 129 equivalent α-carbon atoms. The structural and topological similarity of the subdomains supports the suggestion that GKRP has evolved through a gene duplication and fusion event from an ancestral dimer,[26] similar to other SIS domain-containing proteins,[23] as, for example, GlmS (see below).

The Lid domain consists of a bundle of seven α-helices (αC1−αC7). Its core consists of a triple-helical bundle (αC1, αC2, and αC5) with a ubiquitin-like fold. The core is flanked by the C-terminal αC7 helix that stacks approximately parallel to the central bundle and by helices αC3, αC4, and αC6 that run approximately perpendicular. The Lid domain is initiated by a rather irregular peptide stretch (residues 499−512, termed Linker) in which a short β-hairpin (residues 501−504) is the only secondary structure feature. The 14 Linker residues are wedged between the α-helical bundle that constitutes the core of the Lid domain and the SIS domain dimer and contribute significantly to the Lid−SIS interface.

Surface Mutation. The K326T/K327T double mutation is located on the surface of the SIS-2 domain at the end of helix αB2 (Figure 2B). The region is not involved in contacts with SIS-1 or the active site and does not interact with the Lid domain or the N-terminus. Biochemically, $GKRP_{K326}$ behaves like wild-type GKRP (Figure 1), and one can thus assume that all conclusions drawn from the mutant structure are valid for wild-type GKRP as well. Despite the dramatic improvement that the K326T/K327T double mutation made on crystal quality, there are only modest involvements in crystal contacts: Thr327 is solvent-exposed and not involved in contacts to neighboring molecules at all. The Thr326 side chain is found in two conformations, one of which makes two interactions with a symmetry-related molecule (denoted with an asterisk): a van der Waals interaction of Thr326 CG2 with Asn197* and a hydrogen bond of OG1 to water W283, which in turn contacts Thr198*. It is probable that the native Lys326 side chain cannot be properly accommodated into the observed crystal contact. The K450T/K451T double mutation is located on the solvent-exposed surface of helix αB6 of the SIS-2 domain (Figure 2B). In the $GKRP_{K326}$ crystal lattice, Lys450 is involved in a crystal contact that, presumably, cannot be maintained in $GKRP_{K450}$. Interestingly, the ability of $GKRP_{K450}$ to form a GK−GKRP complex is weakened 3-fold, indicating that this region might be involved in GK binding, albeit not as a key element of the binding interface.

Fructose Phosphate Binding Site. The two fructose phosphate isomers F1P and F6P both act on mammalian GKRPs in a competitive manner with micromolar activities [for rat GKRP, K_d(F6P) = 20 μM and K_d(F1P) = 1 μM] and likely bind to a single binding site.[7,8] GKRP could be crystallized in the presence of F1P and binds in a deeply buried cavity at the junction between the SIS and Linker domains (Figure 3). Clear ligand electron density indicates that β-D-F1P binds in the pyranose configuration at the edge of the β-sheet of the SIS-1 domain (Figures 2C and 3). Within SIS-1, the binding site is formed by the N-terminal regions of helices αA3 (residues 107−110) and αA7 (residues 258 and 259) and one face of helix αA4′ (Glu150 and Glu153), which together line the fructose moiety. The phosphate group is embraced by a loop (residues 179−184) that precedes helix αA5. Terminal phosphate oxygens form hydrogen bonds with Ser110 and Ser179 (hydroxyl groups), Val180 and Gly181 (main chain amino groups), and water molecules (with low *B* factors) tightly bound in the pocket (Figure 3). The N-terminal end of helix αA5 is directed to the phosphate site and may contribute to binding of F1P by dipole−dipole interaction. The binding site is complemented by one helix of SIS-2 (αB3, residues Glu348 and His351) and one edge of the Lid domain (residues 512−518). There, the Lys514 ε-amino group neutralizes one negative charge of the phosphate by interacting with O1P (3.3 Å) and with phosphoester O1 (2.9 Å). Hydroxyl substituents of fructopyranose are involved in polar contacts with residues of SIS-1 (Thr109, backbone NH; Glu153, carboxylate OE1), SIS-2 (Glu348, carboxylate OE2), and the Lid domain (Lys514 NZ, Asn512 ND2) and two water molecules.

Crystals of $GKRP_{K326}$ in complex with phosphate ($GKRP_{K326}$−P) were inadvertently identified when we attempted to crystallize apo-$GKRP_{K326}$. Although the final purification steps as well as the reservoir buffer for

dx.doi.org/10.1021/bi4000782 | *Biochemistry* 2013, 52, 3523−3531

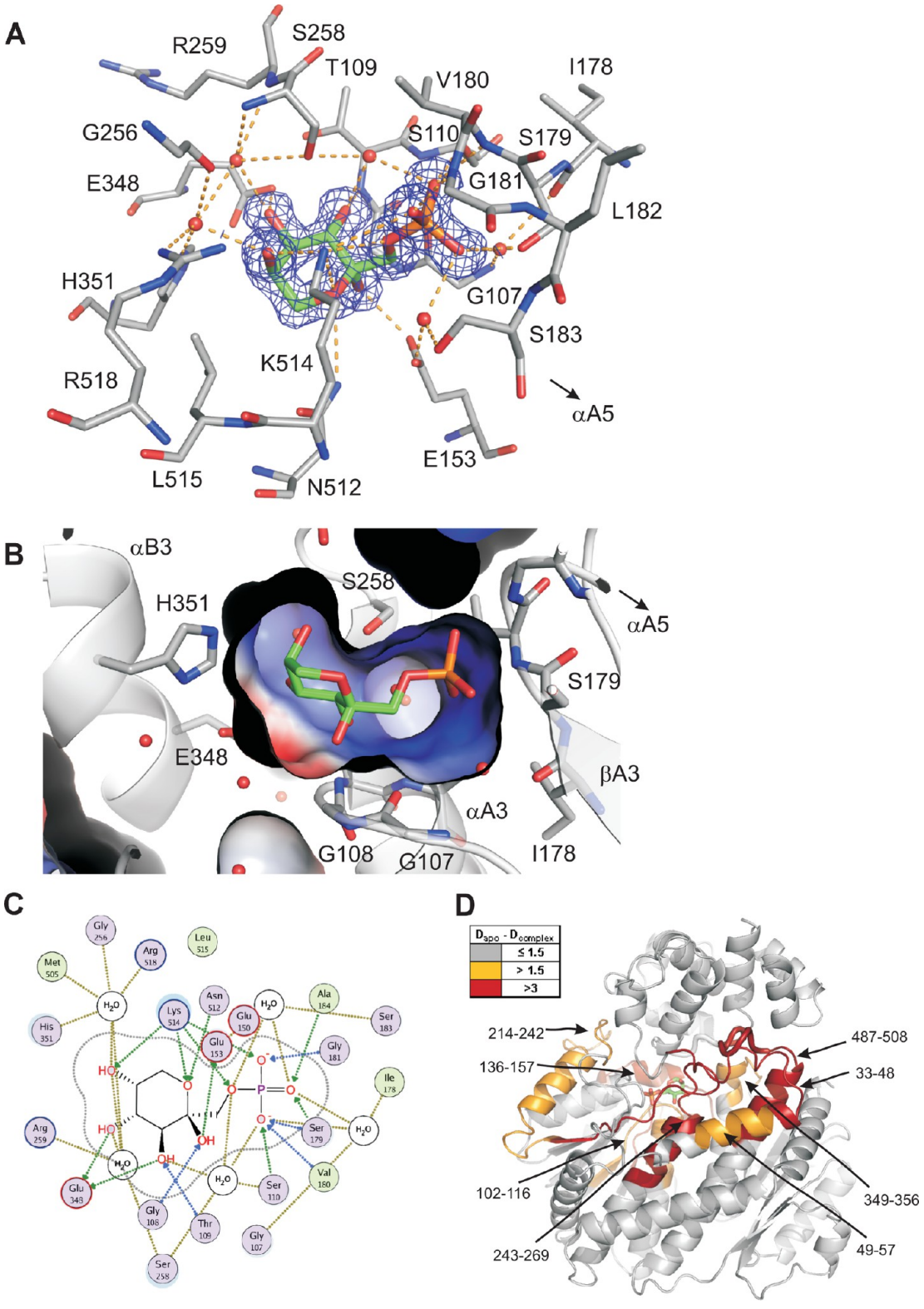

Figure 3. Fructose phosphate binding site. (A) Stick representation of the F1P (green carbon atoms) binding site. Water molecules are shown as red spheres and hydrogen bonds as yellow dotted lines. The final weighted $2|F_o| - |F_c|$ electron density map for F1P is shown as a blue mesh contoured at 1.5σ. (B) Surface plot of the F1P binding site colored according to electrostatic potential (blue for positive and red for negative). (C) Schematic plot of F1P interactions. Hydrogen bonds are shown as dotted arrows (green for side chain and blue for main chain); nonpolar contacts are shown as dotted lines. (D) Protection against H−D exchange due to ligand binding mapped onto the structure. Regions that are protected against deuterium incorporation (after 30 min) in the presence of F1P as compared to apo-GKRP are color-coded by the degree of protection.

crystallization did not contain phosphate salts, there was clear electron density that could be modeled as a phosphate ion (Figure S2 of the Supporting Information). Because the Ni-NTA affinity purification step employed a phosphate buffer, we

dx.doi.org/10.1021/bi4000782 | *Biochemistry* 2013, 52, 3523−3531

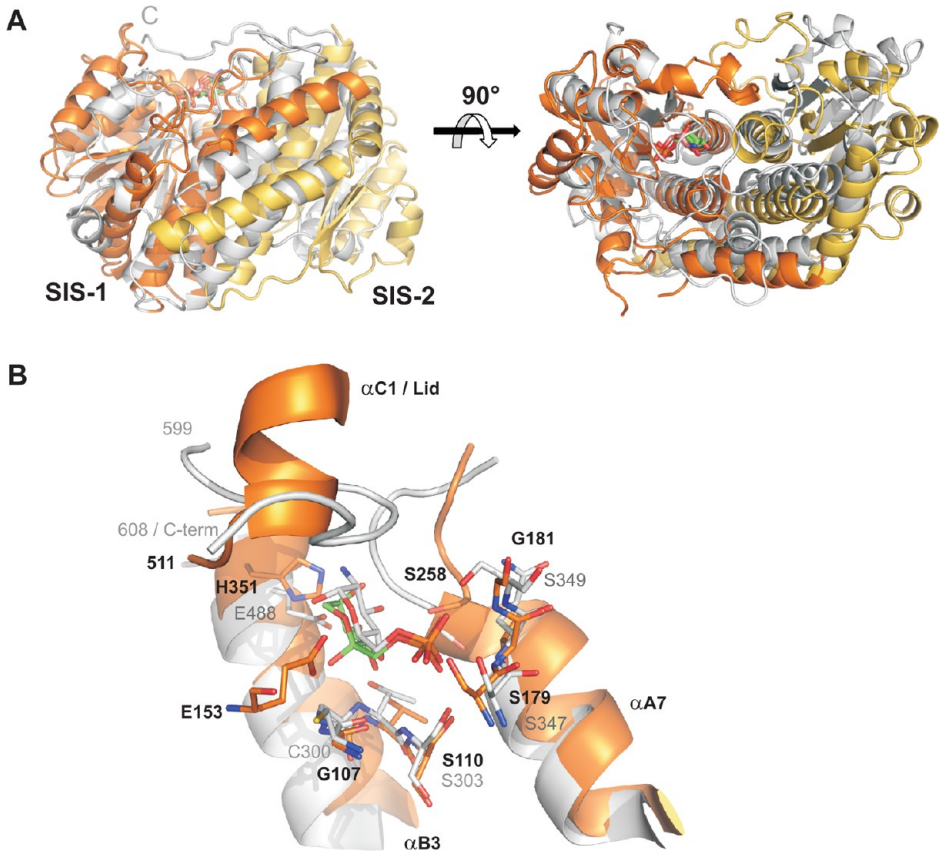

Figure 4. Comparison to GlmS. (A) Ribbon diagram of the GKRP SIS domain dimer (SIS-1 colored orange and SIS-2 colored yellow). The structure of GlmS (gray, PDB entry 1MOQ) is superimposed on the basis of the SIS-1 domains. Ligands F1P (green) and glucosamine 6-phosphate (magenta) are shown as stick models. LID domain and Linker peptide of GKRP have been omitted for the sake of clarity. The C-terminus of GlmS is labelled in gray. (B) Comparison of GKRP (orange, black labels) and GlmS (gray, gray labels) binding sites. Hydrogen bonds, water molecules, and several contacting residues have been omitted for the sake of clarity. Note that GKRP residue Glu153 has no equivalent in GlmS.

assume that residual phosphate remained bound to the protein during the following purification steps. When bound to phosphate instead of F1P, $GKRP_{K326}$ assumes a conformation almost identical to that of the $GKRP_{K326}$–F1P complex (0.14 Å rmsd on all Cα atoms). The lacking sugar moiety is replaced by several water molecules, but apart from that, there are no significant deviations in the active site architecture (Figure S2 of the Supporting Information).

Despite the internal 2-fold symmetry of the SIS domains, GKRP contains only one ligand binding site, namely that in SIS-1, with the bound F1P. Another putative binding site at the equivalent region in SIS-2 is not occupied. A comparable asymmetry is observed in glucosamine-6-phosphate synthase,[25] which also contains a SIS dimer in an arrangement similar to that of GKRP, but only one binding site for the reaction product glucosamine 6-phosphate in its SIS-1 domain (Figure 4).

The observed structure is corroborated by a mutational analysis of fructose phosphate binding.[8] Mutation of residues directly involved in phosphate group binding would be expected to have a profound effect on the binding affinity of fructose phosphates. Accordingly, the three mutations S110A, S179A, and K514A were found to abolish binding or strongly decrease the dissociation constant of both F1P and F6P. The G107C mutation caused a marked increase in F6P affinity, while reducing the affinity for F1P. Presumably, the sulfhydryl side chain of a Cys107 mutant displaces Glu153, which coordinates the anomeric hydroxyl group of F1P, thus weakening binding. F6P in turn has no anomeric hydroxyl in this position and may not be affected by this displacement (Figure 4B and Figure S3A of the Supporting Information) when bound. In contrast, a comparison to GlmS (Figure 4B), which also features a Gly → Cys exchange at this position, indicates that the cysteine side chain may form an additional favorable van der Waals interaction with C6 of F6P. Several other mutants (T337A, T411A, K499A, and D507A) that were probed had only marginal effects on fructose phosphate dissociation constants, in line with their location outside the binding site.

H–D Mapping of the Fructose Phosphate Binding Site. To map the potential ligand binding sites, the amide hydrogen exchange behavior of apo-GKRP was compared to that of ligand-bound GKRP (Figure S4 and Table S1 of the Supporting Information). After H–D exchange for 30 min, nine regions in GKRP show less deuterium incorporation in the presence of either ligand (F6P or F1P) than in the presence of apo-GKRP. Protection against H–D exchange indicates a more stable and less flexible protein fold in the presence of ligand. F6P and F1P show protection against H–D exchange mostly in the same regions in GKRP (Figure S4A of the Supporting Information). Together with biochemical data,[8] this supports the idea that there is one binding site in GKRP for both ligands. Mapping of the H–D exchange results to the crystallographically observed structure indicates four regions (residues 102–116, 136–157, 243–269, and 349–356) that include residues that are engaged in direct interactions with F1P

dx.doi.org/10.1021/bi4000782 | *Biochemistry* 2013, 52, 3523–3531

(Figure 3D) or F6P (Figure S4B of the Supporting Information). Two further peptides (214−242 and 487−508, which includes part of the Linker) do not directly contact F1P but flank its binding site. Residues 33−48 of the N-terminus and adjacent residues 49−57 are probably indirectly stabilized through the contacts of the N-terminus and Lid domain with the fructose phosphates. Subtle differences in the amount of H−D exchange (Figure S4A of the Supporting Information) most probably reflect conformational differences between the two complexes.[16]

CONCLUSION

The high-resolution structure of GKRP in its inactive F1P-bound form confirms earlier suggestions of a SIS domain dimer and reveals additional structural elements that cap the ligand binding site. H−D exchange experiments support the notion that F1P and its antagonist F6P compete for the same binding site but are not sufficiently sensitive to identify larger structural differences between the respective complexes. It is believed that GKRP interacts with the super-open, low-affinity state of GK.[27] The required "active" GKRP state ("active" with respect to GK) is further stabilized by F6P and in turn can abolish GK catalytic activity. F1P, on the other hand, stabilizes an "inactive" GKRP conformation with low affinity for GK.[14] The high-resolution structure of the GKRP−F1P complex provides a starting point for understanding the mechanism of fructose phosphate-dependent GK regulation at an atomic level. In the absence of further structural data, one can only speculate about the exact molecular mechanism of this switch (Supporting Information), but it appears to be reasonable to assume that F6P binding may trigger conformational changes between the individual GKRP domains that ultimately establish the GK binding site.

ASSOCIATED CONTENT

Supporting Information

Supplementary results and discussion, Figures S1−S4, and Table S1. This material is available free of charge via the Internet at http://pubs.acs.org.

Accession Codes

The structures described here have been deposited as PDB entries 4bb9 ($GKRP_{K326}$−F1P) and 4bba ($GKRP_{K326}$−P).

AUTHOR INFORMATION

Corresponding Author

*Boehringer Ingelheim Pharma GmbH & Co. KG, D-88397 Biberach an der Riss, Germany. E-mail: alexander.pautsch@boehringer-ingelheim.com. Telephone: +49 (7351) 54-4683. Fax: +49 (7351) 54-97924.

Notes

The authors declare no competing financial interest.

ABBREVIATIONS

GK, glucokinase; GKRP, glucokinase regulatory protein; $GKRP_{WT-His}$, human, wild-type, full-length GKRP with a C-terminal His_6 tag; $GKRP_{K326}$, $GKRP_{WT-His}$ K326T/K327T double mutant; $GKRP_{K450}$, $GKRP_{WT-His}$ K450T/K451T double mutant; F6P, fructose 6-phosphate; F1P, fructose 1-phosphate; IC_{50}, half-maximal inhibitory concentration; SIRAS, single isomorphous replacement with anomalous signal; SIS, sugar isomerase domain; H−D, hydrogen−deuterium; rmsd, root-mean-square deviation.

REFERENCES

(1) Matschinsky, F. M., et al. (2011) Glucokinase activators for diabetes therapy: May 2010 status report. *Diabetes Care 34* (Suppl. 2), S236−S243.
(2) Zelent, D., et al. (2005) Glucokinase and glucose homeostasis: Proven concepts and new ideas. *Biochem. Soc. Trans. 33*, 306−310.
(3) Petit, P., et al. (2011) The active conformation of human glucokinase is not altered by allosteric activators. *Acta Crystallogr. D67*, 929−935.
(4) Kamata, K., Mitsuya, M., Nishimura, T., Eiki, J., and Nagata, Y. (2004) Structural basis for allosteric regulation of the monomeric allosteric enzyme human glucokinase. *Structure 12*, 429−438.
(5) Lin, S. X., and Neet, K. E. (1990) Demonstration of a slow conformational change in liver glucokinase by fluorescence spectroscopy. *J. Biol. Chem. 265*, 9670−9675.
(6) Matschinsky, F. M. (2009) Assessing the potential of glucokinase activators in diabetes therapy. *Nat. Rev. Drug Discovery 8*, 399−416.
(7) Van Schaftingen, E. (1989) A protein from rat liver confers to glucokinase the property of being antagonistically regulated by fructose 6-phosphate and fructose 1-phosphate. *Eur. J. Biochem. 179*, 179−184.
(8) Veiga-da-Cunha, M., and Van Schaftingen, E. (2002) Identification of fructose 6-phosphate- and fructose 1-phosphate-binding residues in the regulatory protein of glucokinase. *J. Biol. Chem. 277*, 8466−8473.
(9) Toyoda, Y., Tsuchida, A., Iwami, E., Shironoguchi, H., and Miwa, I. (2001) Regulation of hepatic glucose metabolism by translocation of glucokinase between the nucleus and the cytoplasm in hepatocytes. *Horm. Metab. Res. 33*, 329−336.
(10) Sarabu, R., Berthel, S. J., Kester, R. F., and Tilley, J. W. (2011) Novel glucokinase activators: A patent review. *Expert Opin. Ther. Pat. 21*, 13−33.
(11) Shiota, M., Galassetti, P., Monohan, M., Neal, D. W., and Cherrington, A. D. (1998) Small amounts of fructose markedly augment net hepatic glucose uptake in the conscious dog. *Diabetes 47*, 867−873.
(12) Wolff, M., Kauschke, S. G., Schmidt, S., and Heilker, R. (2008) Activation and translocation of glucokinase in rat primary hepatocytes monitored by high content image analysis. *J. Biomol. Screening 13*, 837−846.
(13) Veiga-da-Cunha, M., Courtois, S., Michel, A., Gosselain, E., and Van Schaftingen, E. (1996) Amino acid conservation in animal glucokinases. Identification of residues implicated in the interaction with the regulatory protein. *J. Biol. Chem. 271*, 6292−6297.
(14) Anderka, O., et al. (2008) Biophysical characterization of the interaction between hepatic glucokinase and its regulatory protein: Impact of physiological and pharmacological effectors. *J. Biol. Chem. 283*, 31333−31340.
(15) Brocklehurst, K. J., Davies, R. A., and Agius, L. (2004) Differences in regulatory properties between human and rat glucokinase regulatory protein. *Biochem. J. 378*, 693−697.
(16) Rist, W., Jorgensen, T. J., Roepstorff, P., Bukau, B., and Mayer, M. P. (2003) Mapping temperature-induced conformational changes in the *Escherichia coli* heat shock transcription factor sigma 32 by amide hydrogen exchange. *J. Biol. Chem. 278*, 51415−51421.
(17) Kabsch, W. (2010) XDS. *Acta Crystallogr. D66*, 125−132.
(18) Soding, J., Biegert, A., and Lupas, A. N. (2005) The HHpred interactive server for protein homology detection and structure prediction. *Nucleic Acids Res. 33*, W244−W248.
(19) Sheldrick, G. M. (2010) Experimental phasing with SHELXC/D/E: Combining chain tracing with density modification. *Acta Crystallogr. D66*, 479−485.
(20) Morris, R. J., Perrakis, A., and Lamzin, V. S. (2003) ARP/wARP and automatic interpretation of protein electron density maps. *Methods Enzymol. 374*, 229−244.
(21) Emsley, P., and Cowtan, K. (2004) Coot: Model-building tools for molecular graphics. *Acta Crystallogr. D60*, 2126−2132.
(22) Davis, I. W., et al. (2007) MolProbity: All-atom contacts and structure validation for proteins and nucleic acids. *Nucleic Acids Res. 35*, W375−W383.

(23) Bateman, A. (1999) The SIS domain: A phosphosugar-binding domain. *Trends Biochem. Sci. 24*, 94−95.
(24) Derewenda, Z. S. (2004) Rational protein crystallization by mutational surface engineering. *Structure 12*, 529−535.
(25) Teplyakov, A., Obmolova, G., Badet-Denisot, M. A., Badet, B., and Polikarpov, I. (1998) Involvement of the C terminus in intramolecular nitrogen channeling in glucosamine 6-phosphate synthase: Evidence from a 1.6 Å crystal structure of the isomerase domain. *Structure 6*, 1047−1055.
(26) Veiga-da-Cunha, M., Sokolova, T., Opperdoes, F., and Van Schaftingen, E. (2009) Evolution of vertebrate glucokinase regulatory protein from a bacterial N-acetylmuramate 6-phosphate etherase. *Biochem. J. 423*, 323−332.
(27) Baltrusch, S., and Tiedge, M. (2006) Glucokinase regulatory network in pancreatic β-cells and liver. *Diabetes 55*, S55−S64.